University of Reading

The Indian Easterly Jet During the pre-monsoon season in India

Article

Published Version

Creative Commons: Attribution 4.0 (CC-BY)

Open Access

Croad, H. L., Shonk, J. K. P., Chevuturi, A. ORCID: https://orcid.org/0000-0003-2815-7221, Turner, A. G. ORCID: https://orcid.org/0000-0002-0642-6876 and Hodges, K. I. ORCID: https://orcid.org/0000-0003-0894-229X (2023) The Indian Easterly Jet During the pre-monsoon season in India. Geophysical Research Letters, 50 (23). e2023GL105400. ISSN 0094-8276 doi: 10.1029/2023GL105400 Available at https://centaur.reading.ac.uk/114235/

It is advisable to refer to the publisher's version if you intend to cite from the work. See Guidance on citing.

To link to this article DOI: http://dx.doi.org/10.1029/2023GL105400

Publisher: American Geophysical Union

All outputs in CentAUR are protected by Intellectual Property Rights law, including copyright law. Copyright and IPR is retained by the creators or other copyright holders. Terms and conditions for use of this material are defined in the End User Agreement.

www.reading.ac.uk/centaur

University of Reading

CentAUR

Central Archive at the University of Reading

Reading's research outputs online

Check for updates

Geophysical Research Letters

RESEARCH LETTER
10.1029/2023GL105400

The Indian Easterly Jet During the Pre-Monsoon Season in India

Hannah L. Croad[1], Jonathan K. P. Shonk[2,3], Amulya Chevuturi[2,4], Andrew G. Turner[1,2], and Kevin I. Hodges[1,2]

[1]Department of Meteorology, University of Reading, Reading, UK, [2]National Centre for Atmospheric Science, University of Reading, Reading, UK, [3]Now at MetOffice@Reading, University of Reading, Reading, UK, [4]UK Centre for Ecology & Hydrology, Wallingford, UK

Key Points:

- The Indian Easterly Jet is a thermal wind in the mid-troposphere over India during the pre-monsoon, identified in reanalysis data
- The jet resembles the African Easterly Jet, but is smaller and weaker, and is not associated with significant easterly wave activity
- Interannual variability in jet state is linked to variability in pre-monsoon weather, including surface temperature and precipitation

Supporting Information:

Supporting Information may be found in the online version of this article.

Correspondence to:

H. L. Croad,
h.croad@pgr.reading.ac.uk

Citation:

Croad, H. L., Shonk, J. K. P., Chevuturi, A., Turner, A. G., & Hodges, K. I. (2023). The Indian Easterly Jet during the pre-monsoon season in India. *Geophysical Research Letters*, *50*, e2023GL105400. https://doi.org/10.1029/2023GL105400

Received 10 JUL 2023
Accepted 8 NOV 2023

Author Contributions:

Conceptualization: Jonathan K. P. Shonk, Amulya Chevuturi
Data curation: Amulya Chevuturi
Formal analysis: Hannah L. Croad
Funding acquisition: Jonathan K. P. Shonk
Investigation: Hannah L. Croad
Methodology: Hannah L. Croad, Jonathan K. P. Shonk, Amulya Chevuturi, Andrew G. Turner, Kevin I. Hodges
Project Administration: Jonathan K. P. Shonk, Amulya Chevuturi, Andrew G. Turner

© 2023. The Authors.
This is an open access article under the terms of the Creative Commons Attribution License, which permits use, distribution and reproduction in any medium, provided the original work is properly cited.

Abstract We identify for the first time an Indian Easterly Jet (IEJ) in the mid-troposphere during the pre-monsoon using reanalysis data. The IEJ is weaker and smaller than the African Easterly Jet over West Africa, with a climatological location of 10°N, 60–90°E, 700 hPa, and strength 6–7 m s^{-1} during March–May. The IEJ is a thermal wind associated with low-level meridional gradients in temperature (positive) and moisture (negative), resulting from equatorward moist convection and poleward dry convection. The IEJ is associated with a negative meridional potential vorticity gradient, therefore satisfying the Charney-Stern necessary condition for instability. However, no wave activity is detected, suggesting that the potential for combined barotropic-baroclinic instability is not often realized. IEJ strong (weak) years feature increased (reduced) near-surface temperatures and drier (wetter) conditions over India. This study provides an introduction to the IEJ's role in pre-monsoon dynamics, and a platform for further research.

Plain Language Summary Jets, or concentrated regions of fast-moving winds, can form due to temperature gradients working together with the Earth's rotation. Typically these form in the east/west direction, such as the African Easterly Jet, which is well known over tropical West Africa. Using observation-based data of the atmosphere, we set out to explore whether such a jet exists near India during spring-time (the "pre-monsoon"). The Indian Easterly Jet (IEJ), like its counterpart in West Africa, forms in the lower atmosphere between a south-to-north increasing low-level temperature gradient and a reversed temperature gradient at higher altitudes. But unlike in West Africa, the IEJ breaks down once the summer monsoon begins. We use established methods to show that the IEJ winds have the potential to amplify small cyclonic disturbances, which can develop into larger storms. However, we find that this does not occur commonly. Meanwhile, years in which the IEJ is unusually strong tend to be associated with spring-time conditions in India that are warmer and drier than normal. This first research into the IEJ paves the way for further analysis on its role in the development of heatwaves, severe storms and the monsoon onset.

1. Introduction

Mid-tropospheric easterly jets exist in several tropical regions, the best known being the African Easterly Jet (AEJ). The AEJ is a prominent feature of the boreal summer circulation over West Africa, with easterly winds of ~11 m s^{-1} at 600 hPa and ~15°N (Wu et al., 2009). The AEJ is maintained by two diabatically forced meridional circulations, one associated with dry convection in the Saharan thermal low to the north, and another associated with the deep moist convection in the intertropical convergence zone (ITCZ) to the south (Thorncroft & Blackburn, 1999). A positive meridional temperature gradient extends from the surface to 600 hPa, corresponding to easterly wind shear with height, according to the thermal wind relationship. Above this, the meridional temperature gradient is reversed due to latent heating from deep convection to the south, in contrast to strong radiative cooling above the Sahara. This results in peak easterly winds at 600 hPa.

The AEJ is associated with a negative meridional potential vorticity (PV) gradient (Burpee, 1972; Schubert et al., 1991; Thorncroft & Blackburn, 1999), satisfying a necessary condition for instability of the mean flow (Charney & Stern, 1962). The barotropic and baroclinic instability of the flow supports the development of African Easterly Waves (AEWs) on the AEJ (e.g., Pytharoulis & Thorncroft, 1999; Wu et al., 2012). AEWs are convectively coupled waves initiated by convection (mesoscale convective systems [MCSs]) over terrain in eastern Africa (e.g., Hamilton et al., 2020), before propagating westward and developing along the AEJ (Berry

Supervision: Jonathan K. P. Shonk, Amulya Chevuturi, Andrew G. Turner, Kevin I. Hodges
Writing – original draft: Hannah L. Croad
Writing – review & editing: Hannah L. Croad

& Thorncroft, 2005). AEWs can ultimately undergo tropical cyclogenesis (e.g., Núñez Ocasio et al., 2021), with 61% of North Atlantic tropical cyclones originating from AEWs (Russell et al., 2017).

A mid-tropospheric easterly jet and PV reversal also exists over northern Australia, from December to March, with approximately half the strength of the AEJ (Dickinson & Molinari, 2000). Despite satisfying the Charney-Stern instability condition, AEW-like disturbances were not detected on the jet. This is attributed to the smaller zonal extent of the PV reversal over northern Australia (allowing insufficient time for wave growth), or the lack of upstream orography (Dickinson & Molinari, 2000). However, Berry et al. (2012) found that Australian monsoon weather systems resemble AEWs in that they move along the easterly jet at 700 hPa, although with significantly smaller amplitudes. Furthermore, the African Easterly Jet South (AEJ-S) persists over central Africa from September to November at 10°S (Nicholson & Grist, 2003). The AEJ-S is also smaller and weaker than the AEJ, and is not associated with easterly waves. However, the AEJ-S does play a role in moisture distribution in central Africa; a strong (weak) AEJ-S results in enhanced water vapor divergence (convergence) at mid-levels, resulting in dry (wet) conditions further south (Kuete et al., 2020).

Each easterly jet occurs where there is ocean (or tropical rainforest) equatorward of inland deserts. India shares a similar geographic alignment, with the Thar Desert north of the equatorial Indian Ocean. The shift in India's monsoon circulation can be understood as a change in sign of the meridional temperature gradient (Goswami & Chakravorty, 2017). The pre-monsoon (March–May) is the hottest time of year in India, characterized by intense solar radiation. Sensible heating, in particular over the Tibetan Plateau (Yanai et al., 1992), reverses the low-level meridional temperature gradient from negative to positive (Xavier et al., 2007). During March and April the ITCZ lies over the equatorial Indian Ocean (Mitchell & Wallace, 1992), with latent heat release generating a negative meridional temperature gradient aloft, conducive to a mid-level easterly jet.

This study investigates an easterly jet over India during the pre-monsoon, which we call the "Indian Easterly Jet" (IEJ). We will address the following questions:

1. What are the climatological characteristics of the IEJ?
2. Does the IEJ exhibit instability, and if so does it support easterly waves?
3. How is the IEJ linked with pre-monsoon weather over India?

Although periods of easterly flow and associated heavy rainfall have been investigated previously over pre-monsoon India (Sawaisarje et al., 2019), to the authors' knowledge, this is the first study to consider the climatological easterly wind pattern as a jet.

2. Data and Methods

The main data set used is the fifth-generation European Centre for Medium-Range Weather Forecasts (ECMWF) reanalysis product, ERA5, produced using the Integrated Forecasting System model cycle 41r2 (Hersbach et al., 2017, 2020). The meteorological variables used are horizontal wind components, air temperature, and specific humidity on pressure surfaces with a vertical resolution of 50 hPa in the mid-troposphere, Ertel PV and horizontal wind components on the 315 K isentropic surface, and 2m temperature. All data is interpolated onto a regular 0.25° latitude-longitude grid. We also use Global Precipitation Climatology Project V2.3 monthly-mean precipitation (Adler et al., 2003) with 2.5° horizontal resolution. The period of study is 1979–2018 (40 years).

An IEJ index is defined to capture the strength and spatial extent of the zonal wind. Based on the IEJ climatology (Section 3), the IEJ index is defined as the April standardized mean of easterly zonal wind within a three-dimensional region of 70°–80°E, 0°–20°N, and 500–800 hPa (Figures 1b and 1c). Standardization is applied by subtracting the mean value (-3.19 m s^{-1}) and dividing by the standard deviation (0.65 m s^{-1}). Defining the index in April avoids possible contamination from the monsoon onset in May. It is assumed that the mean IEJ state in April is representative of the jet throughout the pre-monsoon season. The jet index region has a larger spatial extent than the IEJ itself to account for any spatial variability. Strong (weak) jet years are defined as those with an IEJ index below (above) the 25th (75th) percentile.

The Charney and Stern (1962) necessary (but not sufficient) condition for instability of the zonal flow requires a reversal of the meridional PV gradient. As outlined by Hsieh and Cook (2008), under the quasi-geostrophic

19448007, 2023, 23, Downloaded from https://agupubs.onlinelibrary.wiley.com/doi/10.1029/2023GL105400 by Test, Wiley Online Library on [29/11/2023]. See the Terms and Conditions (https://onlinelibrary.wiley.com/terms-and-conditions) on Wiley Online Library for rules of use; OA articles are governed by the applicable Creative Commons License

19448007, 2023, 23, Downloaded from https://agupubs.onlinelibrary.wiley.com/doi/10.1029/2023GL105400 by Test, Wiley Online Library on [29/11/2023]. See the Terms and Conditions (https://onlinelibrary.wiley.com/terms-and-conditions) on Wiley Online Library for rules of use; OA articles are governed by the applicable Creative Commons License

assumption (on pressure surfaces, conservation of PV being approximately equivalent to the conservation of quasi-geostrophic PV [QGPV], q), if the zonal flow is unstable, the Charney-Stern condition requires that:

$$\frac{\partial \bar{q}}{\partial y} = \beta - \frac{\partial^2 \bar{u}}{\partial y^2} - \frac{\partial}{\partial p}\left(\frac{p f_0^{\,2}}{R S_p}\frac{\partial \bar{u}}{\partial p}\right) < 0 \quad (1)$$

where y = meridional distance (m), f_0 = Coriolis parameter (s^{-1}) at fixed latitude (10°N), β = meridional gradient of the Coriolis parameter (s^{-1} m^{-1}), u = zonal wind speed (m s^{-1}), p = pressure (Pa), R = gas constant (287 J kg^{-1} K^{-1}), and $S_p = \left[-\left(\frac{T}{\theta}\right)\frac{\partial \theta}{\partial p}\right]$, where T = temperature (K), θ = potential temperature (K). The overbar refers to the zonal mean. On the RHS, the first term is the meridional gradient of planetary vorticity, which acts to inhibit instability (i.e., is positive). The second and third terms represent how horizontal and vertical shear determine the meridional gradient of q. If the instability condition is satisfied by horizontal and/or vertical shear (i.e., these terms being negative), there is the potential for barotropic and/or baroclinic instability respectively.

Wave activity is investigated using a Fourier bandpass filter applied to the daily 700 hPa meridional wind field. AEWs have a typical period of 2–6 days (Burpee, 1972), but an extended range of 2–10 days is used for this initial investigation.

3. Climatology and Interannual Variability

3.1. Climatology

Over India, the mid-tropospheric zonal wind switches between monsoon westerlies in summer (June–September), and easterlies during the rest of the year (Figure 1a). Peak easterly winds occur during the pre-monsoon (March–May), with a maximum speed of 6–7 m s^{-1} in April, over southern India at 10°N, ~700 hPa (Figure 1b), and 60°–90°E (Figure 1c). This is the IEJ, embedded within a band of easterlies at the same latitude. The IEJ is a local acceleration of the broader easterly flow (in thermal wind balance), positioned over the maximum positive low-level meridional temperature gradient over southern India, which has a greater (smaller) magnitude in strong (weak) jet years (Figure S1 in Supporting Information S1). At monsoon onset, a positive meridional temperature gradient extends through the troposphere, and low-level westerlies are established that overcome the IEJ.

In contrast, over West Africa there is no shift in the mid-tropospheric zonal wind, since the West African monsoon (WAM) is shallower than 600 hPa, allowing easterly winds to persist to the south of 20°N (Figure 1d). Consistent with Wu et al. (2009), peak easterly winds associated with the AEJ occur in July at ~15°N and 600 hPa with strength 11–12 m s^{-1}, above the weak westerlies of the WAM (Figure 1e). The IEJ and AEJ share a similar structure in vertical cross-section (Figures 1b and 1e), both positioned below the Tropical Easterly Jet at ~200 hPa. However, the AEJ is approximately twice as strong as the IEJ, and resides ~100 hPa higher. The AEJ spans 40°W–20°E (Figure 1f), with a zonal extent double that of the IEJ, due to the larger zonal extent of the landmass in West Africa. The AEJ persists for 6 months, whereas the IEJ is only present for 3 months, consistent with the more dynamical zonal wind structure over India.

The climatological background environment of the IEJ and AEJ are presented in Figure 2. Conditions south of the IEJ (0°) are relatively cool and moist, with a surface temperature of 27°C and a quasi-moist adiabatic temperature profile above 900 hPa (Figure 2a). Positive vertical mass-flux values indicate ascent throughout the troposphere (Figure 2b), with mass-flux convergence above 300 hPa, and divergence below (Figure 2c). This is consistent with deep moist convection in the ITCZ over the equatorial ocean, with evaporation below 300 hPa and latent heat release above. North of the IEJ (20°N), the low-level troposphere is hotter and drier, with a surface temperature of 32°C and a dry adiabatic temperature profile between 900 and 600 hPa (Figure 2a). There is ascent below 600 hPa, and descent above this level (Figure 2b), with mass-flux convergence between 850 and 300 hPa (Figure 2c). This demonstrates shallow dry convection over the deserts of north-west India. Hence, diabatic processes play a crucial role in establishing a low-level positive meridional temperature gradient over southern India, which reduces with height and reverses at 680 hPa (Figure 2a). This is conducive to a peak in easterly winds, the IEJ, at 680 hPa.

The atmospheric profiles for the AEJ are similar to those of the IEJ. The low-level troposphere is cool and moist to the south, but hot and dry to the north (Figure 2d). The vertical mass-flux sections indicate ascent and deep moist convection to the south of the AEJ, and shallow dry convection to the north (Figures 2e and 2f), indicating

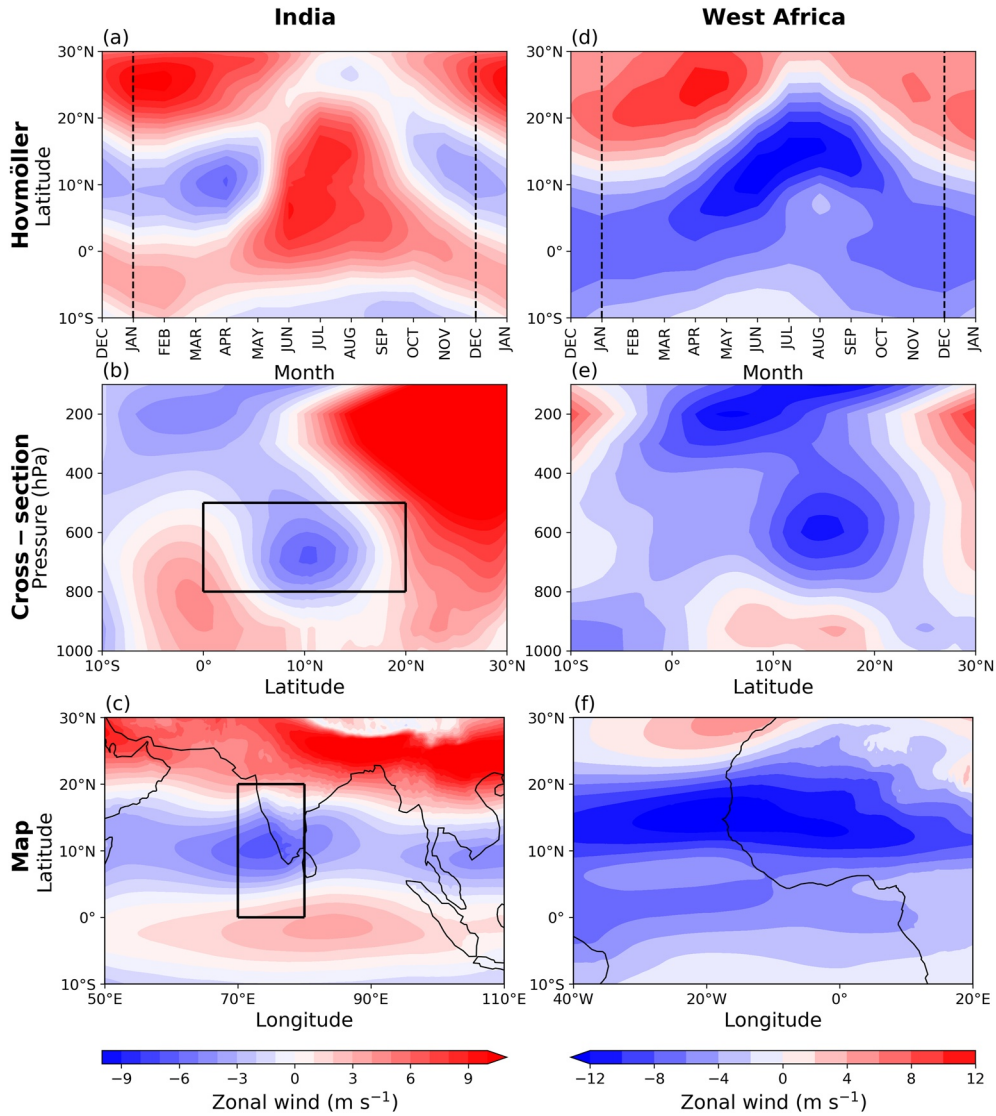

Figure 1. Easterly jet characteristics for (a–c) India and (d–f) West Africa. Climatological zonal wind (shaded), as Hovmöller diagrams averaged over (a) 650–700 hPa, 70°–80°E and (d) 600 hPa, 0°–20°W; latitude-pressure cross-sections averaged over (b) 70°–80°E (April), (e) 0°–20°W (July); maps averaged over (c) 650–700 hPa (April), (f) 600 hPa (July). The black dashed lines in panels (a, d) demarcate the annual cycle. Boxes in panels (b, c) outline the spatial extent of the Indian Easterly Jet index (Section 2).

that the IEJ and AEJ are maintained by the same fundamental processes. However, the deep moist convection over West Africa is stronger (indicated by larger positive vertical mass-flux magnitudes), and the regions of deep moist convection and shallow dry convection are more meridionally constrained (Figure 2e). This is consistent with a stronger low-level temperature gradient over West Africa, with a surface temperature of 26°C at 10°N and 33°C at 20°N (i.e., a larger temperature difference over a smaller meridional extent). This is facilitated by a stronger negative moisture gradient over West Africa (Figure 2d), and explains the AEJ's greater strength.

3.2. Interannual Variability

The IEJ index time series highlights considerable interannual variability over the study period, with no notable trend (Figure 3a). Weak jet years exhibit larger deviations from the mean than strong jet years. In particular, the IEJ was extremely weak in 1997, with an index value 3 standard deviations away from the mean. Since a strong El Niño occurred in 1997–1998, it was investigated whether the IEJ state was linked with the El Niño-Southern

19448007, 2023, 23, Downloaded from https://agupubs.onlinelibrary.wiley.com/doi/10.1029/2023GL105400 by Test, Wiley Online Library on [29/11/2023]. See the Terms and Conditions (https://onlinelibrary.wiley.com/terms-and-conditions) on Wiley Online Library for rules of use; OA articles are governed by the applicable Creative Commons License

19448007, 2023, 23, Downloaded from https://agupubs.onlinelibrary.wiley.com/doi/10.1029/2023GL105400 by Test, Wiley Online Library on [29/11/2023]. See the Terms and Conditions (https://onlinelibrary.wiley.com/terms-and-conditions) on Wiley Online Library for rules of use; OA articles are governed by the applicable Creative Commons License

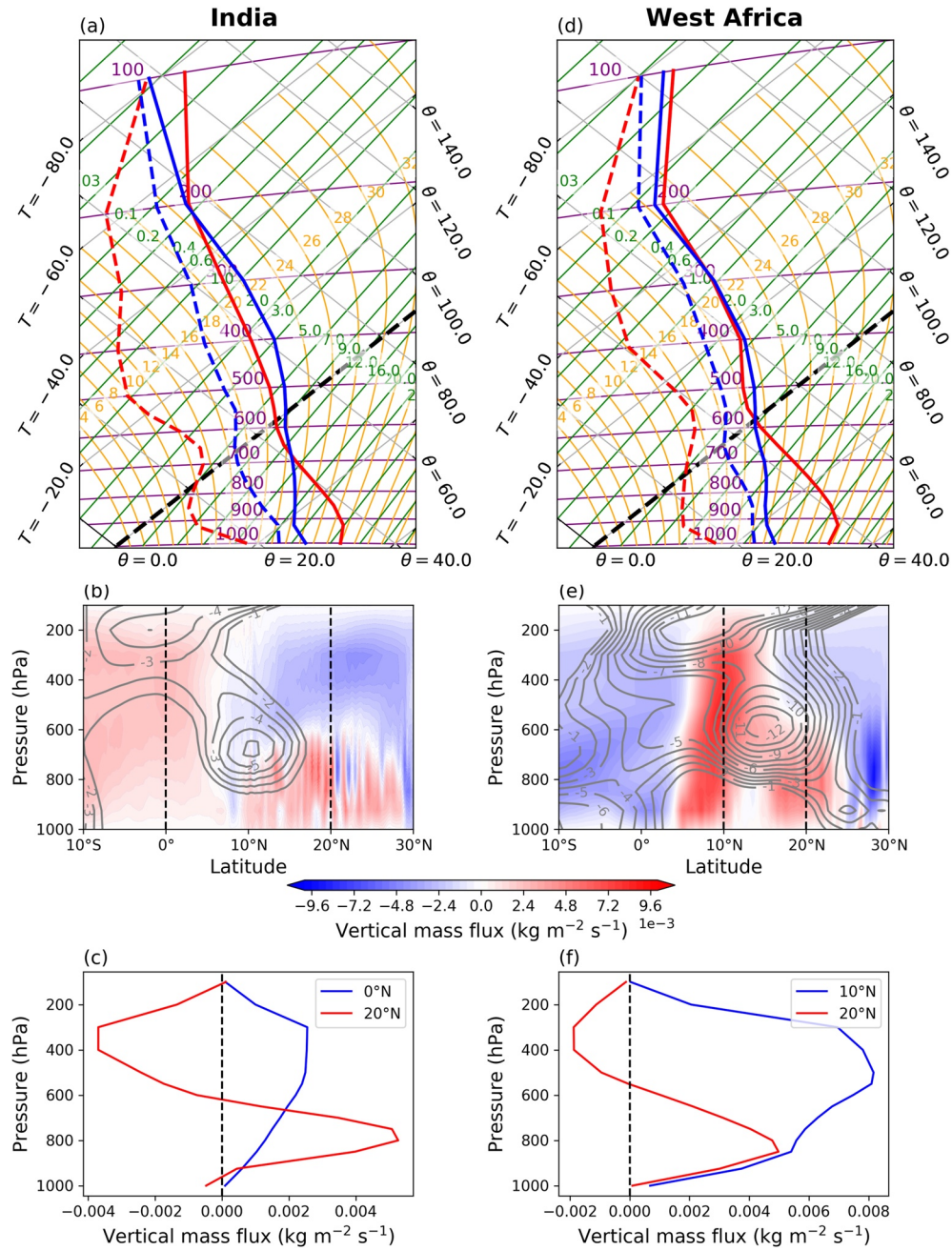

Figure 2. Tephigrams (top) and vertical mass-flux (middle and bottom), over India (a–c, April 70°–80°E average) and West Africa (d–f, July 0°–20°W average), with emphasis on profiles at (a–c) 0°and 20°N, and (d–f) 10° and 20°N. (a, d) Climatological profiles of temperature (solid lines) and dewpoint temperature (dashed lines) to the south (blue) and north (red) of the jets. (b, e) Vertical cross-sections of climatological vertical mass-flux (shading), with the chosen latitudes marked by black vertical dashed lines and easterly zonal wind (gray contours) overlaid. (c, f) Profiles of the vertical mass-flux at the south (blue) and north (red) latitudes.

Oscillation. However, correlating the IEJ index with the Oceanic Niño Index did not yield a statistically significant result (Figure S2 in Supporting Information S1).

A preliminary examination to determine whether the IEJ state is related to the Madden-Julian Oscillation (MJO; Figure S3 in Supporting Information S1) yielded no definitive link. This is likely because the IEJ index has been defined as a monthly average, and the MJO varies over days to weeks. However, Figure S3 in Supporting Information S1 does show that a strong IEJ is associated with a ∼10% greater chance of weak MJO activity. Such a

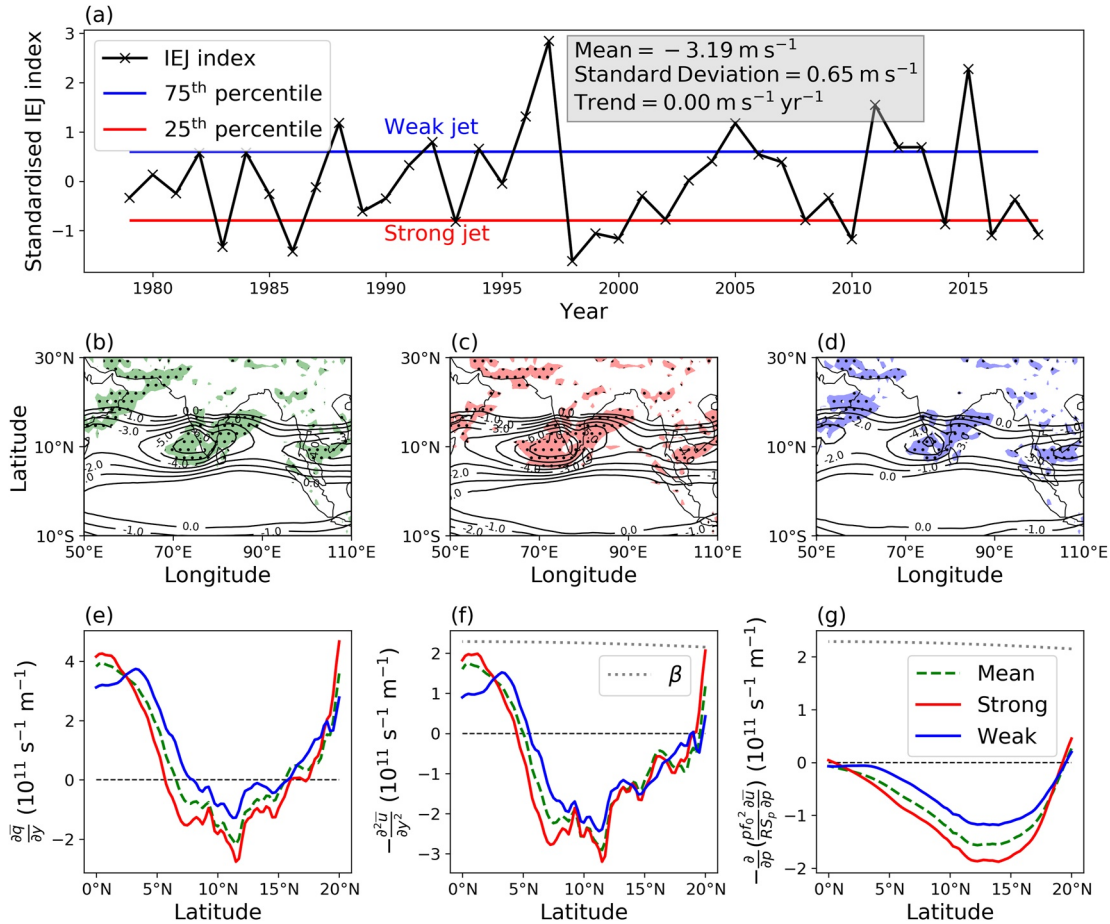

Figure 3. (a) The Indian Easterly Jet (IEJ) index (black) time series, with 25th (red) and 75th (blue) percentiles marked. Summary statistics of the IEJ index before standardization are contained in the gray inset. (b–d) Regions on the 315 K isentropic surface with negative meridional Ertel potential vorticity gradient (colored stippling) and easterly zonal wind (contours), averaged in April for (b) the climatological mean, (c) strong, and (d) weak year composites. (e–g) Terms from Equation 1 averaged over 650–700 hPa and 70°–80°E, (e) $\frac{\partial \bar{q}}{\partial y}$, (f) $-\frac{\partial^2 \bar{u}}{\partial y^2}$ (smoothed by 2° latitude moving-average), and (g) $-\frac{\partial}{\partial p}\left(\frac{\rho {f_0}^2}{R S_p}\frac{\partial \bar{u}}{\partial p}\right)$, for the 1979–2018 mean (green dashed lines), strong year composite (red solid lines), and weak year composite (blue solid lines). β is overlaid (gray dotted line) in panels (f, g).

link could be investigated in future work, given the known association between seasonally integrated measures of MJO amplitude and tropical weather (Vellinga & Milton, 2018).

4. Instability and Waves

4.1. Instability

Regions with a negative meridional PV gradient are shaded over contours of easterly zonal wind on the 315 K isentropic surface in Figures 3b–3d. In the climatological mean (Figure 3b), the PV reversal spans a broad region over southern India, collocated with the IEJ core and extending northeastward. Hence, the climatological IEJ satisfies the Charney and Stern (1962) condition of instability. The PV reversal spans a larger zonal extent when the IEJ is strong (Figure 3c), but is smaller and patchier in weak years (Figure 3d).

Consistent with this, the meridional QGPV gradient is negative from ~7°–16°N, with a larger (smaller) meridional extent in strong (weak) IEJ years (Figure 3e). The negative meridional QGPV gradient is a consequence of both the horizontal (Figure 3f) and vertical (Figure 3g) shear terms being negative, indicating the potential for combined barotropic-baroclinic instability.

The horizontal shear term (Figure 3f) is negative from ~6°–20°N, and is alone sufficient to satisfy the instability condition (i.e., $\beta - \frac{\partial^2 \bar{u}}{\partial y^2} < 0$) near the jet core. Furthermore, the Kuo (1949) necessary condition for barotropic

19448007, 2023, 23, Downloaded from https://agupubs.onlinelibrary.wiley.com/doi/10.1029/2023GL105400 by Test, Wiley Online Library on [29/11/2023]. See the Terms and Conditions (https://onlinelibrary.wiley.com/terms-and-conditions) on Wiley Online Library for rules of use; OA articles are governed by the applicable Creative Commons License

19448007, 2023, 23, Downloaded from https://agupubs.onlinelibrary.wiley.com/doi/10.1029/2023GL105400 by Test, Wiley Online Library on [29/11/2023]. See the Terms and Conditions (https://onlinelibrary.wiley.com/terms-and-conditions) on Wiley Online Library for rules of use; OA articles are governed by the applicable Creative Commons License

instability is satisfied where $\beta - \frac{\partial^2 \bar{u}}{\partial y^2} = 0$. This occurs on the cyclonic side of the flow for the climatological mean and strong jet composite at 9.5° and 7°N respectively, indicating potential hotspots for barotropic instability. The vertical shear term (Figure 3g) is negative from 0° to 20°N, and therefore contributes to the negative meridional QGPV gradient, indicating the potential for baroclinic instability. The magnitude of the vertical shear term is slightly smaller than the horizontal shear term (i.e., $\beta - \frac{\partial}{\partial p}\left(\frac{p f_0^2}{R S_p}\frac{\partial \bar{u}}{\partial p}\right) > 0$ everywhere), indicating that horizontal shear is more dominant.

Hence, the IEJ has the potential for combined barotropic-baroclinic instability. That the horizontal and vertical shear terms are more negative in strong years than weak years (Figures 3e–3g) suggests that this potential for instability is greatest when the jet is strong.

4.2. Wave Activity

Since the IEJ exhibits the potential for combined barotropic-baroclinic instability, it is possible that the jet could support the growth of easterly waves. However, an investigation using a 2–10 days bandpass filter did not demonstrate any significant signals of wave activity associated with the IEJ (Figure S4 in Supporting Information S1), unlike the AEJ.

The absence of AEW-like disturbances on the IEJ can likely be attributed to the small zonal extent of the reversed PV gradient (~2,500 km compared to ~5,000 km over West Africa), like the jet over northern Australia (Dickinson & Molinari, 2000). Furthermore, there is a lack of upstream orography (the East Ghats upstream have an average elevation of only ~600 m), which is known to be important for the development of AEWs on the AEJ (Hamilton et al., 2020). Previous studies have also shown that to maintain and grow easterly waves, interactions with MCSs are crucial (e.g., Núñez Ocasio et al., 2020). Hence, the lack of wave activity is likely linked to the fact that the strong IEJ (i.e., when the jet is most dynamically unstable) is associated with reduced convection over India. Berry et al. (2012) found that Australian monsoon weather systems propagate along the 700 hPa easterly jet over northern Australia. However, this cannot be the case for the IEJ, since the jet disappears at monsoon onset.

5. Pre-Monsoon Meteorology

The IEJ index is significantly correlated with the 2m temperature over India and parts of South Asia (Figure 4a). A strong IEJ corresponds to warm surface temperature anomalies of ~1.0°C over India (Figure 4b), whilst weak IEJ years are associated with anomalously cool conditions, with surface temperature anomalies of −1.2°C (Figure 4c). Hence, weak IEJ years can be more than 2.0°C cooler than strong IEJ years over much of India. The weak composite is statistically different from climatology (95% confidence level) over much of the country, whereas the strong composite is only statistically different over central India.

Furthermore, the IEJ has a significant correlation with precipitation over India during the pre-monsoon (Figure 4d). During the pre-monsoon, India is mainly dry with climatological precipitation of less than 2 mm day^{-1}. During strong (weak) IEJ years, there is less (more) precipitation (Figures 4e and 4f) with suppressed (enhanced) convection (Figure S5 in Supporting Information S1). During strong IEJ years the largest precipitation anomalies occur in the Bay of Bengal, with anomalies exceeding −1.2 mm day^{-1}, extending westwards over India where conditions are up to 0.8 mm day^{-1} drier than climatology (Figure 4e). The suppression of convection and precipitation in strong IEJ years is statistically different from climatology in the Bay of Bengal, but not over India. In contrast, the enhanced precipitation during weak IEJ years is statistically significant over India, with conditions 0.8–1.2 mm day^{-1} wetter than climatology (Figure 4f). The largest contrast occurs over the southern tip of India, where conditions during strong IEJ years can be ~1.8 mm day^{-1} drier than weak IEJ years.

Moisture flux transport over the region is examined as in Kuete et al. (2020). The net zonal moisture transport (NZMT; kg m^{-2} s^{-1}) is computed as the difference between moisture flux across the western (70°E) and eastern (80°E) boundary of the jet: NZMT = $(\rho uh)_W - (\rho uh)_E$ where ρ = water density (1,000 kg m^{-3}) and h = specific humidity (kg kg^{-1}). Positive (negative) values indicate moisture flux convergence (divergence). The climatological IEJ is associated with a region of mid-tropospheric moisture flux divergence at 10°N and 700 hPa (Figure 4g). This moisture flux divergence is intensified when the jet is strong, consistent with drier conditions over the region (Figure 4h). In contrast, there is anomalous moisture flux convergence in weak IEJ years, favoring enhanced

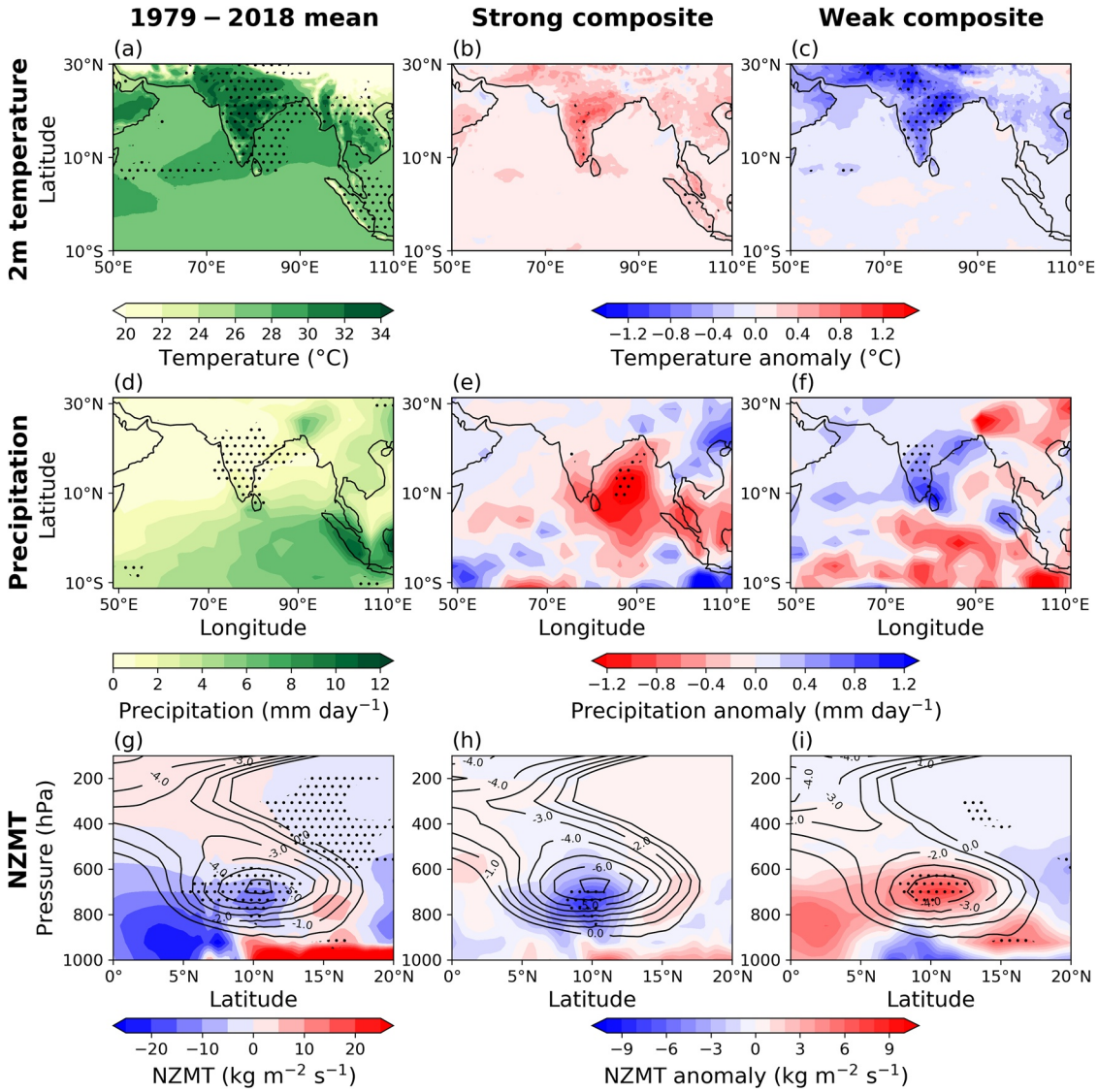

Figure 4. (a) Climatological April 2 m temperature (shaded), and regions where the Pearson correlation with the Indian Easterly Jet index is statistically significant at the 95% confidence level (stippling). (b) Strong and (c) weak anomaly composites for April 2 m temperature (shaded) relative to the 1979–2018 April mean, and regions where the composite is statistically different from the 1979–2018 April mean at the 95% confidence level according to a Student *t*-test (stippling). Subplots (d–f) and (g–i) are the same as (a–c) but for precipitation and net zonal moisture transport, respectively. Easterly zonal wind composite contours are overlain in panels (g–i). Variables were linearly detrended at each gridpoint to remove any climate trends.

precipitation over India (Figure 4i). This suggests a possible mechanism by which the IEJ feeds back on precipitation and the large-scale environment during the pre-monsoon.

6. Conclusions and Discussion

In this study we have investigated the IEJ, a mid-tropospheric easterly jet over India during the pre-monsoon season, using reanalysis data. The IEJ, like the AEJ over West Africa, is maintained by equatorward moist convection and poleward dry convection, although the IEJ is weaker and smaller. Like the AEJ, the IEJ satisfies the Charney-Stern necessary condition for instability, with the flow exhibiting the potential for combined barotropic-baroclinic instability. However, no wave activity was detected. That the potential for instability is not realized is likely related to the small zonal extent of the jet, and the lack of upstream topography. The differences in jet characteristics are likely grounded in the strength of the monsoon systems with which each jet is associated. The AEJ occurs during the WAM season, because the associated positive meridional temperature

19448007, 2023, 23, Downloaded from https://agupubs.onlinelibrary.wiley.com/doi/10.1029/2023GL105400 by Test, Wiley Online Library on [29/11/2023]. See the Terms and Conditions (https://onlinelibrary.wiley.com/terms-and-conditions) on Wiley Online Library for rules of use; OA articles are governed by the applicable Creative Commons License

19448007, 2023, 23, Downloaded from https://agupubs.onlinelibrary.wiley.com/doi/10.1029/2023GL105400 by Test, Wiley Online Library on [29/11/2023]. See the Terms and Conditions (https://onlinelibrary.wiley.com/terms-and-conditions) on Wiley Online Library for rules of use; OA articles are governed by the applicable Creative Commons License

gradient does not extend in depth beyond the mid-troposphere. However, the Indian summer monsoon is stronger and more expansive than the WAM, with a positive meridional temperature gradient established throughout the troposphere. Hence, the IEJ cannot exist after monsoon onset. The IEJ more closely resembles the weaker and smaller-scale easterly jets over northern Australia and central Africa.

The IEJ has been linked with the meteorology of pre-monsoon India. The results are consistent with the thermal wind: increased (reduced) near-surface temperatures and drier (wetter) conditions over India during strong (weak) IEJ years contribute to strengthened (weakened) positive temperature and negative moisture meridional gradients, and therefore a stronger (weaker) jet. The IEJ may also feed back on the large-scale environment via moisture transport, with enhanced moisture flux divergence (convergence) when the jet is strong (weak). Understanding this feedback should be the subject of future study.

The question arises as to whether the IEJ can act as a useful indicator of weather conditions over India. Since the IEJ state is strongly correlated with temperature, precipitation, and convection over India, future work could investigate the link between the jet state and heatwave and thunderstorm events, the main meteorological hazards during the pre-monsoon. Chiefly, heatwaves might be more likely during strong IEJ years when conditions are hotter and drier. An investigation of the higher frequency (e.g., daily) variability of the jet is required to understand whether the IEJ can provide a useful indicator, for example, investigating any link between the IEJ state and the MJO. Future work should also look at whether the IEJ has an impact beyond the pre-monsoon (e.g., impacting monsoon onset).

Data Availability Statement

ECMWF ERA5 reanalysis data is publicly available and can be downloaded from the Copernicus Climate Change Service (C3S) Climate Data Store (Hersbach et al., 2017). The Global Precipitation Climatology Project V2.3 data (Adler et al., 2003) from 1979 to present is provided by the National Oceanic and Atmospheric Administration (NOAA) Physical Sciences Laboratory (PSL), Boulder, Colorado, USA, and is freely available from their website at https://psl.noaa.gov/data/gridded/data.gpcp.html. The NOAA Climate Prediction Center Ocean Niño Index data set (NOAA, 2020) from 1950 to present is freely available at https://climatedataguide.ucar.edu/climate-data/nino-sst-indices-nino-12-3-34-4-oni-and-tni. The NOAA Interpolated Outgoing Longwave Radiation data (Liebmann & Smith, 1996) from 1974 to present is provided by the NOAA PSL, Boulder, Colorado, USA, and is freely available from their website at https://psl.noaa.gov/data/gridded/data.interp_OLR.html. The Real-Time Multivariate MJO Index derived from Wheeler and Hendon (2004), based on satellite-derived OLR and zonal winds at 850 and 200 hPa from NCEP reanalysis data sets, is provided by the Australian Bureau of Meteorology (BOM, 2023), and is freely available from their website (http://www.bom.gov.au/climate/mjo/).

Acknowledgments
Hannah L. Croad was supported by the Undergraduate Research Opportunities Programme (UROP) scheme at the University of Reading. Jonathan K. P. Shonk was supported by NERC Grant NE/N018591/1. Andrew G. Turner was support by NERC Grant NE/S004890/1. Amulya Chevuturi and Kevin I. Hodges were funded as part of the NERC National Centre for Atmospheric Science.

References

Adler, R. F., Huffman, G. J., Chang, A., Ferraro, R., Xie, P.-P., Janowiak, J., et al. (2003). The version-2 global precipitation climatology project (GPCP) monthly precipitation analysis (1979–present). *Journal of Hydrometeorology*, *4*(6), 1147–1167. https://doi.org/10.1175/1525-7541(2003)004<1147:TVGPCP>2.0.CO;2

Berry, G. J., Reeder, M. J., & Jakob, C. (2012). Coherent synoptic disturbances in the Australian monsoon. *Journal of Climate*, *25*(24), 8409–8421. https://doi.org/10.1175/JCLI-D-12-00143.1

Berry, G. J., & Thorncroft, C. (2005). Case study of an intense African easterly wave. *Monthly Weather Review*, *133*(4), 752–766. https://doi.org/10.1175/mwr2884.1

BOM. (2023). Real-time multivariate MJO index (1974-present) [Dataset]. Retrieved from http://www.bom.gov.au/climate/mjo/graphics/rmm.74toRealtime.txt

Burpee, R. W. (1972). The origin and structure of easterly waves in the lower troposphere of North Africa. *Journal of the Atmospheric Sciences*, *29*(1), 77–90. https://doi.org/10.1175/1520-0469(1972)029<0077:TOASOE>2.0.CO;2

Charney, J. G., & Stern, M. (1962). On the stability of internal baroclinic jets in a rotating atmosphere. *Journal of the Atmospheric Sciences*, *19*(2), 159–172. https://doi.org/10.1175/1520-0469(1962)019<0159:OTSOIB>2.0.CO;2

Dickinson, M., & Molinari, J. (2000). Climatology of sign reversals of the meridional potential vorticity gradient over Africa and Australia. *Monthly Weather Review*, *128*(11), 3890–3900. https://doi.org/10.1175/1520-0493(2001)129<3890:COSROT>2.0.CO;2

Goswami, B., & Chakravorty, S. (2017). Dynamics of the Indian summer monsoon climate. In *Oxford research encyclopedia of climate science*. https://doi.org/10.1093/acrefore/9780190228620.013.613

Hamilton, H., Núñez Ocasio, K., Evans, J., Young, G., & Fuentes, J. (2020). Topographic influence on the African easterly jet and African easterly wave energetics. *Journal of Geophysical Research: Atmospheres*, *125*(8), e2019JD032138. https://doi.org/10.1029/2019jd032138

Hersbach, H., Bell, B., Berrisford, P., Hirahara, S., Horányi, A., Muñoz-Sabater, J., et al. (2017). Complete ERA5 from 1940: Fifth generation of ECMWF atmospheric reanalyses of the global climate [Dataset]. Copernicus Climate Change Service (C3S) Climate Data Store (CDS). https://doi.org/10.24381/cds.143582cf

Hersbach, H., Bell, B., Berrisford, P., Hirahara, S., Horányi, A., Muñoz-Sabater, J., et al. (2020). The ERA5 global reanalysis. *Quarterly Journal of the Royal Meteorological Society*, *146*(730), 1999–2049. https://doi.org/10.1002/qj.3803

Hsieh, J.-S., & Cook, K. H. (2008). On the instability of the African easterly jet and the generation of African waves: Reversals of the potential vorticity gradient. *Journal of the Atmospheric Sciences*, *65*(7), 2130–2151. https://doi.org/10.1175/2007JAS2552.1

Kuete, G., Mba, W. P., & Washington, R. (2020). African easterly Jet South: Control, maintenance mechanisms and link with southern subtropical waves. *Climate Dynamics*, *54*(3–4), 1539–1552. https://doi.org/10.1007/s00382-019-05072-w

Kuo, H.-L. (1949). Dynamic instability of two-dimensional nondivergent flow in a barotropic atmosphere. *Journal of Meteorology*, *6*(2), 105–122. https://doi.org/10.1175/1520-0469(1949)006<0105:DIOTDN>2.0.CO;2

Liebmann, B., & Smith, C. A. (1996). Description of a complete (interpolated) outgoing longwave radiation dataset. *Bulletin America Meteorology Social*, *77*(6), 1275–1277. Retrieved from http://www.jstor.org/stable/26233278

Mitchell, T. P., & Wallace, J. M. (1992). The annual cycle in equatorial convection and sea surface temperature. *Journal of Climate*, *5*(10), 1140–1156. https://doi.org/10.1175/1520-0442(1992)005<1140:TACIEC>2.0.CO;2

Nicholson, S. E., & Grist, J. P. (2003). The seasonal evolution of the atmospheric circulation over West Africa and equatorial Africa. *Journal of Climate*, *16*(7), 1013–1030. https://doi.org/10.1175/1520-0442(2003)016<1013:TSEOTA>2.0.CO;2

NOAA. (2020). Ocean Niño index from climate prediction center (1950-present) [Dataset]. NOAA Physical Science Laboratory. Retrieved from https://climatedataguide.ucar.edu/climate-data/nino-sst-indices-nino-12-3-34-4-oni-and-tni

Núñez Ocasio, K. M., Brammer, A., Evans, J. L., Young, G. S., & Moon, Z. L. (2021). Favorable monsoon environment over eastern africa for subsequent tropical cyclogenesis of African easterly waves. *Journal of the Atmospheric Sciences*, *78*(9), 2911–2925. https://doi.org/10.1175/jas-d-20-0339.1

Núñez Ocasio, K. M., Evans, J. L., & Young, G. S. (2020). A wave-relative framework analysis of AEW–MCS interactions leading to tropical cyclogenesis. *Monthly Weather Review*, *148*(11), 4657–4671. https://doi.org/10.1175/mwr-d-20-0152.1

Pytharoulis, I., & Thorncroft, C. (1999). The low-level structure of African easterly waves in 1995. *Monthly Weather Review*, *127*(10), 2266–2280. https://doi.org/10.1175/1520-0493(1999)127<2266:TLLSOA>2.0.CO;2

Russell, J. O., Aiyyer, A., White, J. D., & Hannah, W. (2017). Revisiting the connection between African easterly waves and Atlantic tropical cyclogenesis. *Geophysical Research Letters*, *44*(1), 587–595. https://doi.org/10.1002/2016gl071236

Sawaisarje, G., Khare, P., Chaudhari, H. S., Puviarasan, N., & Ranalkar, M. (2019). Easterly wave activity and associated heavy rainfall during the pre-monsoon season of 2005. *Meteorology and Atmospheric Physics*, *131*(3), 313–327. https://doi.org/10.1007/s00703-017-0575-0

Schubert, W. H., Ciesielski, P. E., Stevens, D. E., & Kuo, H.-C. (1991). Potential vorticity modeling of the ITCZ and the Hadley circulation. *Journal of the Atmospheric Sciences*, *48*(12), 1493–1509. https://doi.org/10.1175/1520-0469(1991)048<1493:PVMOTI>2.0.CO;2

Thorncroft, C., & Blackburn, M. (1999). Maintenance of the African easterly jet. *Quarterly Journal of the Royal Meteorological Society*, *125*(555), 763–786. https://doi.org/10.1002/qj.49712555502

Vellinga, M., & Milton, S. F. (2018). Drivers of interannual variability of the east African "long rains". *Quarterly Journal of the Royal Meteorological Society*, *144*(712), 861–876. https://doi.org/10.1002/qj.3263

Wheeler, M. C., & Hendon, H. H. (2004). An all-season real-time multivariate MJO index: Development of an index for monitoring and prediction. *Monthly Weather Review*, *132*(8), 1917–1932. https://doi.org/10.1175/1520-0493(2004)132<1917:aarmmi>2.0.co;2

Wu, M.-L. C., Reale, O., Schubert, S. D., Suarez, M. J., Koster, R. D., & Pegion, P. J. (2009). African easterly jet: Structure and maintenance. *Journal of Climate*, *22*(17), 4459–4480. https://doi.org/10.1175/2009JCLI2584.1

Wu, M.-L. C., Reale, O., Schubert, S. D., Suarez, M. J., & Thorncroft, C. D. (2012). African easterly jet: Barotropic instability, waves, and cyclogenesis. *Journal of Climate*, *25*(5), 1489–1510. https://doi.org/10.1175/2011JCLI4241.1

Xavier, P. K., Marzin, C., & Goswami, B. N. (2007). An objective definition of the Indian summer monsoon season and a new perspective on the ENSO–monsoon relationship. *Quarterly Journal of the Royal Meteorological Society*, *133*(624), 749–764. https://doi.org/10.1002/qj.45

Yanai, M., Li, C., & Song, Z. (1992). Seasonal heating of the Tibetan Plateau and its effects on the evolution of the Asian summer monsoon. *Journal of the Meteorological Society of Japan. Ser. II*, *70*(1B), 319–351. https://doi.org/10.2151/jmsj1965.70.1B_319

19448007, 2023, 23, Downloaded from https://agupubs.onlinelibrary.wiley.com/doi/10.1029/2023GL105400 by Test, Wiley Online Library on [29/11/2023]. See the Terms and Conditions (https://onlinelibrary.wiley.com/terms-and-conditions) on Wiley Online Library for rules of use; OA articles are governed by the applicable Creative Commons License